STRUCTURAL INVESTIGATIONS OF NATURAL AND SYNTHETIC CHLORITE MINERALS BY X-RAY DIFFRACTION, MÖSSBAUER SPECTROSCOPY AND SOLID-STATE NUCLEAR MAGNETIC RESONANCE

Åsa Zazzi[1], Tomas K. Hirsch[2,†], Ekaterina Leonova[2], Andrei Kaikkonen[2], Jekabs Grins[3], Hans Annersten[4] and Mattias Edén[2,*]

[1] Department of Chemistry, Royal Institute of Technology, SE-100 44 Stockholm, Sweden
[2] Physical Chemistry Division, Arrhenius Laboratory, Stockholm University, SE-106 91 Stockholm, Sweden
[3] Inorganic Chemistry Division, Arrhenius Laboratory, Stockholm University, SE-106 91 Stockholm, Sweden
[4] Department of Earth Sciences, Uppsala University, SE-752 36 Uppsala, Sweden

Abstract—The structures of one synthetic and two natural chlorites of the chlinochlore type were explored using X-ray diffraction, magic-angle spinning nuclear magnetic resonance (NMR) and Mössbauer spectroscopy. Rietveld refinements indicated that all structures are of the trioctahedral ordered *IIb* polytype. Mössbauer spectra provided the ratio $^{II}Fe/^{III}Fe$ but gave no evidence for the presence of ^{III}Fe in the brucite-like sheet. We also report unit-cell parameters, Mössbauer isomeric shifts, ^{29}Si NMR chemical shifts as well as ^{27}Al isotropic shifts and quadrupolar coupling parameters. Very broad ^{29}Si NMR peaks from the natural samples prevented us from obtaining accurate information on the Si-Al ordering in the tetrahedral sheets; the limitations of ^{29}Si NMR as applied to natural chlorites are discussed. High-resolution 3QMAS NMR resolved the ^{27}Al signal of the *M4* octahedral site in the brucite-like sheet from the other three Al signals of crystallographically inequivalent octahedral positions.

Key Words—^{27}Al NMR, Cation Distributions, Chlorite, Layered Mineral, Mineral Structure, Mössbauer Spectroscopy, ^{29}Si NMR, XRD.

INTRODUCTION

Chlorites represent a group of phyllosilicate minerals which occur in varying geological sites and which show similar chemical, physical and crystallographic properties (Klein, 2002). Careful diffraction studies and specific chemical analysis are required to distinguish different members of the group, which includes, for example, chamosite, orthochamosite, clinochlore and pennantite (Bailey, 1988). Chlorite minerals occur in sedimentary and low-grade metamorphic rocks, usually present as alteration products in diagenetic classic sediments and as retrograde minerals in metamorphic rocks. Their flexible chemical composition leads to a wide stability range from 70ºC to >700ºC.

The generic structure of phyllosilicate minerals comprises different arrangements of sheets built by cations in octahedral and tetrahedral coordination. For a 1:1 phyllosilicate, an octahedral sheet is linked to one tetrahedral sheet, whereas for 2:1 silicates, the octahedral sheet is linked to two tetrahedral sheets. Another subgrouping criterion is based on the occurrence of di- or trioctahedral phyllosilicates. For the dioctahedral minerals, only two thirds of the octahedral positions are filled by trivalent cations, whereas the trioctahedral ones have full occupancy of octahedral positions. Each tetrahedron shares three oxygens with adjacent tetrahedra, and one oxygen with three octahedra. Substitution of Al for Si leads to an excess of negative charge distributed over the tetrahedral sheets. This may be compensated for either by substituted cations in the octahedral sheet or by hydrated interlayer cations.

Chlorites possess an additional structural complexity (Figure 1), as the 2:1 talc-like sheets alternate with an octahedral brucite-like [$Mg(OH)_2$] sheet (Klein, 2002; Nagy, 1995). The family of chlorite minerals has the generic formula (Brindley and Brown, 1984; Newman and Brown, 1987)

$$(R^{2+}_{6-y-z}R^{3+}_y \square_z)_2(Si_{4-k}R^{3+}_k)_2O_{20}(OH)_{16} \qquad (1)$$
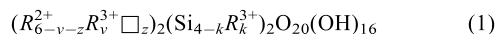
where the parameters y and k denote the degree of substitution of trivalent cations in the octahedral and tetrahedral sheets, respectively, and z accounts for vacancies $\square$ (Foster, 1962). In general, the cation distribution of divalent (R^{2+}) and trivalent (R^{3+}) ions is not known *a priori*, either within each layer or between them. Nevertheless, the net formula (equation 1) may schematically be decomposed into contributions from the two types of alternating layers: the composition of the brucite-like sheet conforms to the formula

* E-mail address of corresponding author:
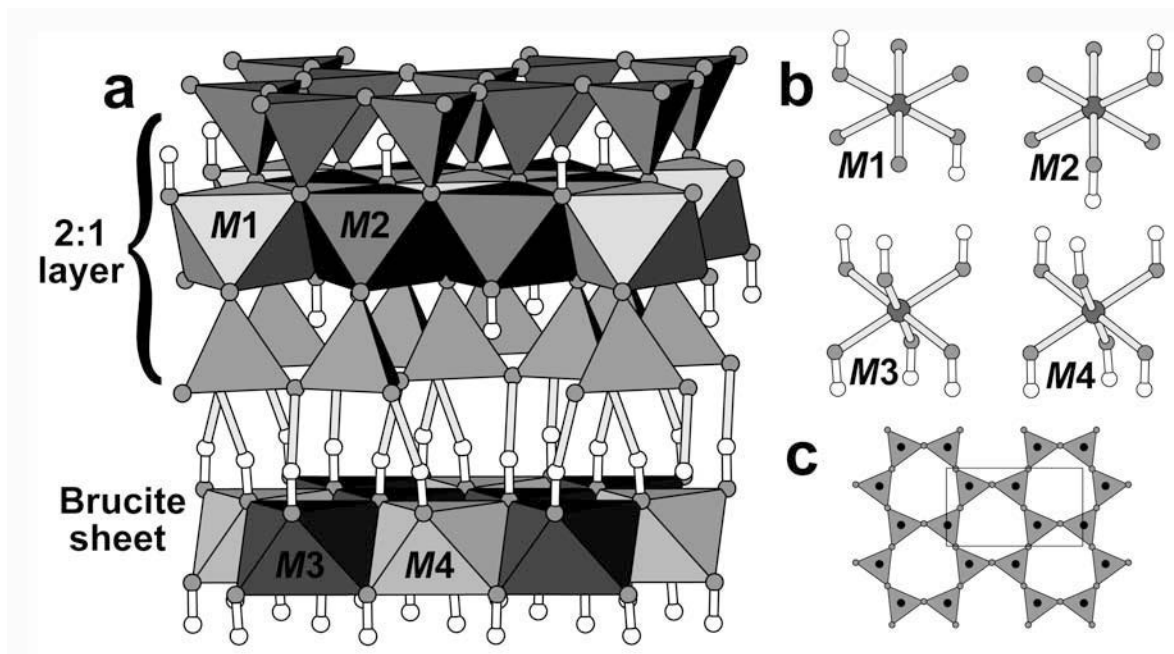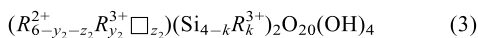mattias@physc.su.se

252

Figure 1. (a) Illustration of the *II*b-4 polytype chlorite structure, with H atoms shown as unfilled circles. (b) The coordination of oxygen atoms and hydroxyl groups around each of the four octahedral *M* sites. Note that *M*1 and *M*2 have hydroxyl groups in *trans* and *cis* configuration, respectively. (c) Illustration of a tetrahedral sheet, viewed along the *c* axis, with the unit-cell outlined.

$$(R_{6-y_1-z_1}^{2+} R_{y_1}^{3+} \square_{z_1})(OH)_{12} \ , \qquad (2)$$
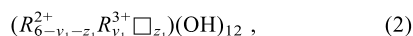
whereas the generic composition of the 2:1 layer is

$$(R_{6-y_2-z_2}^{2+} R_{y_2}^{3+} \square_{z_2})(Si_{4-k} R_k^{3+})_2 O_{20}(OH)_4 \qquad (3)$$

and the coefficients combine as $y_1 + y_2 = y$ and $z_1 + z_2 = z$. R^{3+} in the tetrahedral sheets is usually Al^{3+}; however, other cations may also often be present. There are also wide-range substitutions in the octahedral sheets by divalent ions, such as Fe^{2+} and Mg^{2+}, and trivalent ions, usually Al^{3+} and Fe^{3+}.

Chlorites that are trioctahedral in both the 2:1 layer and in the brucite-like sheet are the most common type found in nature: examples include clinochlore, chamosite and penninite (Bailey, 1988). They differ in the nature of the dominant divalent octahedral cation; Mg^{2+} in clinochlore, Fe^{2+} in chamosite and Mn^{2+} in penninite. The negative charges in the tetrahedral sheets are compensated for by positive charges of the brucite-like sheet and the octahedral sheet of the 2:1 layer. It is, however, difficult to separate the contribution of the two different positively charged layers from each other (Bailey, 1988).

In general, the largest amount of information about an average crystal structure is provided by X-ray diffraction (XRD) techniques. In the absence of suitable single crystals, however, one is restricted to powder data that gives less accurate information, despite the success of the Rietveld method. The structures of lamellar solids, like chlorites, exhibit a considerable degree of randomness, which is manifested, for example, as disorder in the

stacking sequence of layers. This gives rise to intensity distributions in a powder pattern that are very difficult to model due to the deviations from the corresponding ideal ordered structure. Using ordinary laboratory equipment, it is generally only possible to assess the phase purity, unit-cell data and, to some extent, identify the polytype.

The crystal chemistry of chlorites was reviewed by Bailey *et al.* (1971). Among the ordered one-layer chlorites, the *II*b-4 polytype is by far the most abundant in nature and also the only one that has been synthesized. The ideal space group symmetry for chlorite is $C\bar{1}$. In the 2:1 layer there are two octahedral sites, *M*1 and *M*2. The centrosymmetric *M*1 site has a multiplicity of two and is coordinated by four oxygen atoms and two hydroxyl groups in *trans* configuration (Figure 1b), while the non-centrosymmetric *M*2 site has a multiplicity of four and the two hydroxyl groups are in *cis* configuration. The brucite-like sheet also contains two different octahedral sites, both coordinated by six hydroxyl groups (Figure 1b): *M*4, which is centrosymmetric and has a multiplicity of two; and *M*3, non-centro-symmetric and with a multiplicity of four.

The chlorite crystal chemistry has also been characterized together with other phyllosilicates in the work by Newman and Brown (1987) which comprises a summary of several chlorites using a variety of different techniques; X-ray and electron diffraction, infrared spectroscopy and X-ray fluorescence. Brandt *et al.* (2003) used XRD for identification of possible impurities in chlorite samples, together with scanning electron microscopy (SEM) and microprobe analysis. The latter was used for determina-

tion of the average chemical composition, and the ratio of Fe^{2+}/Fe^{3+} was obtained from titration of a dissolved chlorite sample. X-ray *d* values and intensities in chlorite have been determined (Bailey, 1980; Bailey *et al.*, 1971; Moore and Reynolds, 1997). In the study by Moore and Reynolds (1997), the relative intensities of the 00*l* series of reflections were used to determine the heavier elements and their distribution over silicate and hydroxide sites.

Solid-state NMR has been applied extensively to the identification of ^{29}Si and ^{27}Al coordination environments in minerals. The nomenclature $Q^3(mAl)$ specifies a SiO_4 tetrahedron bonded to $mAlO_4$ and to $(3-m)$ silicate units. The ^{29}Si chemical shift of a $Q^3(mAl)$ unit is related to its number of neighbouring Al tetrahedra. The relative abundance of $Q^3(mAl)$ units in a tetrahedral sheet is therefore often directly accessible through the relative intensities of the corresponding ^{29}Si NMR peaks. Focusing on 2:1 phyllosilicates, a $Q^3(0Al)$ Si nucleus resonates in the range from -90 to -98.5 ppm (Mägi *et al.*, 1984; Sanz and Serratosa, 1984; Weiss *et al.*, 1987). When Al substitutes for Si, the ^{29}Si peak position typically gets $4-6$ ppm deshielded for each Al neighbor entering (Mägi *et al.*, 1984). Generally, further deshielding of ^{29}Si chemical shifts in phyllosilicates result from distortions of the tetrahedral sheet, as it tends to shrink its lateral dimensions to conform better to the smaller octahedral sheet. Qualitative correlations have been established between the extent of ^{29}Si deshielding and the excess negative charge introduced by Al substitution, *i.e.* on the ratio $^{IV}Al/(Si+^{IV}Al)$ (Weiss *et al.*, 1987). Typical ^{27}Al isotropic chemical shifts in 2:1 phyllosilicates are $0-12$ ppm for Al in octahedral coordination and $70-77$ ppm in tetrahedral coordination (Lippmaa *et al.*, 1986; Sanz and Serratosa, 1984; Smith, 1993).

An accurate analysis of the distribution of Si and Al in the tetrahedral sheets requires that the various $Q^3(mAl)$ peaks are resolved in the ^{29}Si spectrum. This is usually not a problem for highly ordered silicates, from which ^{29}Si peak widths in magic-angle spinning (MAS) spectra are typically <3 ppm. Unfortunately, from phyllosilicates exhibiting Si-Al disorder, line widths generally range over $10-20$ ppm, leading to spectral overlap. As chlorites exhibit atomic disorder in the tetrahedral sheets and often also contain large amounts of paramagnetic species such as Fe^{2+} (up to several wt.%), they offer substantial challenges for structural characterization by solid-state NMR. Inherent to NMR acquisitions of such samples are that the signals may be significantly broadened, sometimes beyond detection (Grimmer *et al.*, 1983; Morris *et al.*, 1990; Oldfield *et al.*, 1983). The broadening is due to extremely fast nuclear spin-lattice relaxation, caused by the dipolar interactions between the nuclear spins and the unpaired electrons of the paramagnetic sites. As a result, relatively few NMR studies of natural chlorites are reported in the literature and then only for scattered
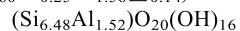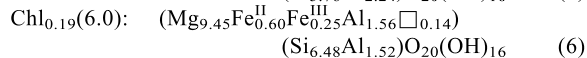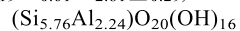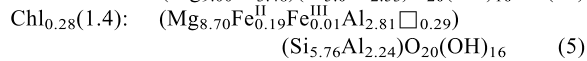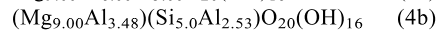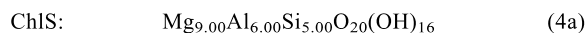
mineral phases of unknown composition or purity (Komarneni *et al.*, 1986; Nakata *et al.*, 1986; Watanabe *et al.*, 1983; Weiss *et al.*, 1987). The greatest insight into Al-Si ordering in the tetrahedral sheets is currently provided by the excellent study of Welch *et al.* (1995), who explored composition-dependent trends in ^{27}Al and ^{29}Si MAS spectra of two synthetic chlorites of the chlinochlore type with no Fe or other paramagnetic ions. Their results will be discussed in relation to our ^{29}Si NMR studies of natural, Fe-containing, chlorites.

The chemical composition of a mineral sample does not reveal the atomic ordering within the different layers. Also, as the composition of a mineral is dependent on its surrounding environments, its history of formation, as well as on the chemistry of the site of formation, a wide diversity among different chlorite specimens may result, necessitating investigations of a large number of samples before overall trends can be ascertained. Using a combination of XRD, Mössbauer and solid-state NMR techniques applied to one synthetic Fe-free chlorite and two natural samples with different compositions of tetrahedral and octahedral ions, this study is intended as a step towards a better understanding of the chlorite structure. While several Mössbauer studies have been carried out on natural chlorites (see Lougear *et al.* (2000), and references therein), very few NMR parameters have been reported for pure chlorites. This investigation therefore also aims to provide a set of ^{29}Si and ^{27}Al chemical shifts and quadrupolar coupling parameters to complement the few existing reports and to serve as benchmark values for future studies.

MATERIALS AND METHODS

The chlorite samples

Our study involved two natural chlorites of different origins (Table 1) as well as one synthetic sample, devoid of Fe and labeled 'ChlS'. It was produced from SiO_2, γ-Al_2O_3 and MgO in a hydrothermal bomb at 1.2 kb and 650ºC for 7 weeks. The detailed synthesis scheme is discussed by Ferrow and Roots (1989). Our investigations started with four natural chlorites, of which two were impure and consequently discarded. The compositions, listed according to increasing Fe content, were determined as:

ChlS: $Mg_{9.00}Al_{6.00}Si_{5.00}O_{20}(OH)_{16}$ (4a)
          $(Mg_{9.00}Al_{3.48})(Si_{5.0}Al_{2.53})O_{20}(OH)_{16}$ (4b)

$Chl_{0.28}(1.4)$: $(Mg_{8.70}Fe^{II}_{0.19}Fe^{III}_{0.01}Al_{2.81}\square_{0.29})$
          $(Si_{5.76}Al_{2.24})O_{20}(OH)_{16}$ (5)

$Chl_{0.19}(6.0)$: $(Mg_{9.45}Fe^{II}_{0.60}Fe^{III}_{0.25}Al_{1.56}\square_{0.14})$
          $(Si_{6.48}Al_{1.52})O_{20}(OH)_{16}$ (6)

Throughout this paper, each natural chlorite sample is labeled according to $Chl_x(y)$, where *y* is the Fe_2O_3 content in wt.% and *x* represents the atomic percentage of Al in the tetrahedral sheets: $x = n_{Al}/(n_{Al} + n_{Si})$. As

Table 1. Indexing and origin of the chlorites used in this study.

Sample	Origin	Source	Catalog number	Color
ChlS	Synthetic	–	–	White
$Chl_{0.28}(1.4)$	Flagstaff Hill, USA	Source Clays Repository, Universisty of Missouri, Columbia, USA	CCa-2(3)	Light green
$Chl_{0.19}(6.0)$	Taberg, Sweden	Swedish Museum of Natural History, Stockholm, Sweden	89530	Green to dark green

ChlS was only available in a limited amount (~60 mg), its chemical composition was not determined: equation 4a provides its nominal composition, assuming no losses during synthesis. As discussed in a later section, the distribution of Al over octahedral and tetrahedral sites were obtained from their respective integrated ^{27}Al NMR signal intensities resulting in the formula equation 4b. In the notation used for the natural samples, ChlS corresponds to $Chl_{0.34}(0.0)$.

The chemical compositions of the natural chlorites were determined by the inductively coupled plasma-atomic emission spectroscopy (ICP-AES) technique at Analytica AB (Luleå, Sweden). Prior to the analysis, samples were dried at 105ºC and fused in a carbon crucible with a flux (lithium metaborate) at 1000ºC. After fusing, the samples were cooled, leading to the formation of a 'bead', which was subsequently dissolved in dilute HNO_3 and used for ICP-AES measurements.

From the resulting wt.% values of oxides (given in Table 2), the stoichiometric coefficients of equations 5 and 6 were determined using a least-squares fitting procedure based on the structural model of equation 1, keeping the constraint that the sum of positive charges per unit formula is 56. The distributions of cations between tetrahedral and octahedral positions were determined by assuming the following: (1) all eight tetrahedral positions are occupied and the chlorites are trioctahedral in both the 2:1 layer and the brucite-like sheet. The XRD results discussed in the next section supported this assumption. (2) Si and Mg are exclusively in tetrahedral and octahedral coordination, respectively, while the Mössbauer data presented below indicate Fe only in octahedral positions. (3) The remaining tetrahedral sites not occupied by Si are filled by Al. (4) The remaining Al were placed in octahedral positions.

Electropositive elements present in minute amounts (<0.3 wt.% oxide content) were unaccounted for in the calculations leading to equations 5 and 6. However, we verified that essentially identical sets of stoichiometric coefficients were also obtained when taking all elements into account in the computations.

The good agreement between the analyzed oxide contents and the corresponding calculated values using the stoichiometric coefficients in formulae 5 and 6 is shown in Table 2. Here, the estimated cation percentages are expressed as oxides involving a total of 28 oxygens instead of 36 as in equation 1: the latter are distributed among 16 hydroxyl and 20 oxide groups. Note that the oxide wt.% will therefore not add up to 100%, as they do not account for the 16 hydroxyl groups. This is sometimes referred to as loss on ignition.

The elemental compositions were also analyzed in a SEM by energy dispersive X-ray micro-analysis. Twelve measurements ascertained that each sample was homogenous, with the average elemental composition in agreement with the results of the ICP analysis.

Powder X-ray diffraction

X-ray diffraction powder photographs were taken using a focusing camera of Guinier-Hägg type with subtraction geometry, $CuK\alpha_1$ radiation, single-coated films, and Si as internal standard. The films were measured by means of a micro-densitometer (Johansson et al., 1980). Rietveld refinements were performed using the program FULLPROF (Rodriguez-Carjaval, 2002).

Mössbauer spectroscopy

The Fe/Fe^{3+} ratio of the natural chlorites was determined by ^{57}Fe Mössbauer spectroscopy, at room temperature, measuring in transmission mode using a

Table 2. Chemical composition (wt.%) of the natural chlorites as analyzed and calculated.

% TS	SiO_2	Al_2O_3	Fe_2O_3	MgO	CaO	K_2O	P_2O_5	TiO_2	MnO_2	Na_2O
$Chl_{0.28}(1.4)$										
Analyzed	30.7	22.9	1.42	31.1	<0.09	0.063	0.011	0.25	0.014	<0.05
Calculated	31.1	23.1	1.37	31.5						
$Chl_{0.19}(6.0)$										
Analyzed	33.6	13.7	5.95	32.9	<0.01	0.680	0.007	0.011	0.134	<0.05
Calculated	34.3	13.8	5.96	33.5						

vibrator in conjunction with a computer. The acceleration of the drive system has a 'saw shape': the two mirror symmetric spectra recorded were folded and subjected to least-squares fitting to Lorenztian lineshapes. The orientation of the chlorite flakes were mounted at a 54.7º angle to the γ beam to avoid textural effects on the absorption doublets (Ericsson and Wäppling, 1976). Calibration of the velocity scale was made from α-Fe at room temperature. Collection of data using 512 channels took 1−2 days depending on the Fe content of the chlorites. Separation of the absorption doublet of the different types of Fe is done readily from the fitted Mössbauer isomer shifts. Fe^{2+}/Fe^{3+} ratios were calculated from the fitted areas under the absorption doublets assuming similar recoil-free fractions of Fe at the different sites.

Solid-state NMR spectroscopy

^{29}Si and ^{27}Al MAS NMR experiments were carried out on finely ground samples using Varian/Chemagnetics Infinity-200 and 400 spectrometers operating at 4.7 T and 9.4 T, respectively. Throughout this work, we used the frequency sign conventions of Levitt (1997), giving the following Larmor frequencies: ^{29}Si: 39.77 MHz at 4.7 T and 79.505 MHz at 9.4 T and ^{27}Al: −104.28 MHz at 9.4 T. Chemical shifts are reported in deshielding (δ) units of ppm, measured relative to tetramethylsilane (TMS) and 1 M $Al(NO_3)_3$ aqueous solution as external references for ^{29}Si and ^{27}Al, respectively. The reported spinning frequencies were stable within 10 Hz throughout the acquisitions. All reported ^{29}Si and ^{27}Al spectra were recorded in the absence of ^{1}H decoupling. We verified for each sample that no substantial improvement in resolution resulted from applying decoupling under our experimental conditions.

^{29}Si NMR. At 9.4 T, the ^{29}Si acquisitions were conducted using filled 6 mm zirconia pencil rotors with spinning rates between 7 and 8 kHz; 4 mm rotors spinning at 12.0 kHz were employed for all measurements at 4.7 T. Due to the large amounts of paramagnetic species in these samples, spin-lattice relaxation times were in the order of tens to hundreds of milliseconds and fully quantitative signals were obtained using 90º pulses with 2 s pulse delays for $Chl_{0.28}(1.4)$, and 0.5 s for $Chl_{0.19}(6.0)$. Zero-filling and exponential apodization of the time-signals were employed prior to Fourier transformation, amounting to an additional 100 Hz Lorentzian broadening of the spectra acquired at 9.4 T, whereas no apodization was applied when processing the time signals acquired at 4.7 T. Due to the limited amount of sample available, no attempts were made to record ^{29}Si spectra of the ChlS specimen.

^{27}Al NMR. ^{27}Al MAS experiments were conducted at 9.4 T, using 3.2 mm rotors spun at 22 kHz, except for ChlS, which was packed in a 4 mm rotor and spun at 10.99 kHz. Short and intense pulses, at a pulse flip angle of ~10º as measured with respect to $Al^{3+}_{(aq)}$, were employed to ensure quantitative 1D MAS spectra, using the same pulse delays as in the corresponding ^{29}Si acquisitions of the natural chlorites and 25 s for ChlS. Zero-filling and additional Lorentzian line broadening (0−200 Hz) were applied in the spectral processing.

2D triple-quantum magic-angle-spinning (3QMAS) experiments (Frydman and Harwood, 1995) were performed at 9.4 T on $Chl_{0.28}(1.4)$ (spinning at 22.4 kHz), $Chl_{0.19}(6.0)$ (14.00 kHz spinning) and ChlS (10.99 kHz). The 3QMAS versions used are described in detail by Brown and Wimperis (1997) and by Massiot *et al.* (1996). 'Shifted-echo'-type experiments were employed, and in the case of the natural chlorites the 'split-t_1' version was used. Typical acquisition conditions were as follows: triple-quantum excitation was performed with a continuous pulse of duration 3−4 µs and ~50 kHz nutation frequency with respect to $Al^{3+}_{(aq)}$. One block of FAM pulses was used for triple-quantum to single-quantum conversion (Madhu *et al.*, 1999), with pulse and inter-pulse delays both set to ~1.2 µs.

RESULTS AND DISCUSSION

Powder XRD

X-ray diffraction indicated a pure ChlS sample (Figure 2a). For the natural specimens $Chl_{0.28}(1.4)$ and $Chl_{0.19}(6.0)$, powder patterns were recorded from different pieces of the mineral samples. For $Chl_{0.28}(1.4)$, some patterns indicated a phase pure sample (Figure 2b), while others contained one observable reflection from SiO_2 (quartz) at $d = 3.345$ Å, with a maximum relative intensity of 9%. For $Chl_{0.19}(6.0)$, the powder pattern (Fig. 2c) contained three very weak extra reflections in the region 2θ = 34−37º. The two natural samples can be regarded as essentially mono-mineralic.

The quality of the powder patterns were diminished by a high background from fluorescence of Fe in the natural samples. Furthermore, the observed asymmetry and broadening of several low-angle peaks indicated crystal imperfections. Reliable unit-cell parameters could not be obtained by an ordinary indexing of the patterns, which yielded unit-cells with very low reliability indices, *e.g.* $M(20) <10$. Unit-cell parameters were therefore determined using the Rietveld method, by simultaneously refining the cell parameters and the unit-cell parameter of the added Si standard. In the Rietveld refinements, atomic co-ordinates in space group $C\bar{1}$ were taken from Joswig *et al.* (1980) for the *IIb*-4 stacking type (Bailey, 1988). A refinement of two different types of parameters was found to significantly improve the fit with observed intensities: (1) the site occupancy factors for the three types of cation sites (octahedral and tetrahedral sites in the 2:1 layer, and the octahedral sites in the brucite-like sheet) and (2) a preferred orientation parameter, with the preferred orientation
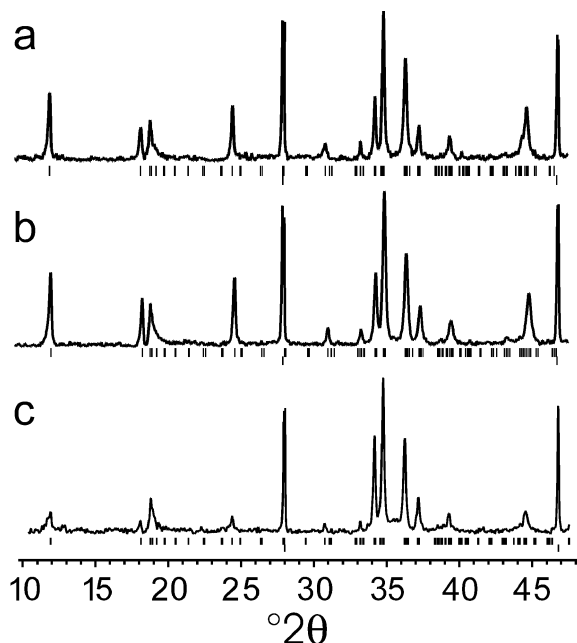
Figure 2. XRD powder patterns of (a) ChlS, (b) $Chl_{0.28}(1.4)$ and (c) $Chl_{0.19}(6.0)$, with reflection markers corresponding to the refined unit-cells given in Table 3. Si was used as the internal standard: its corresponding peaks are indicated by the lower set of markers. They have been truncated in order to obtain a clearer view of the chlorite peaks.
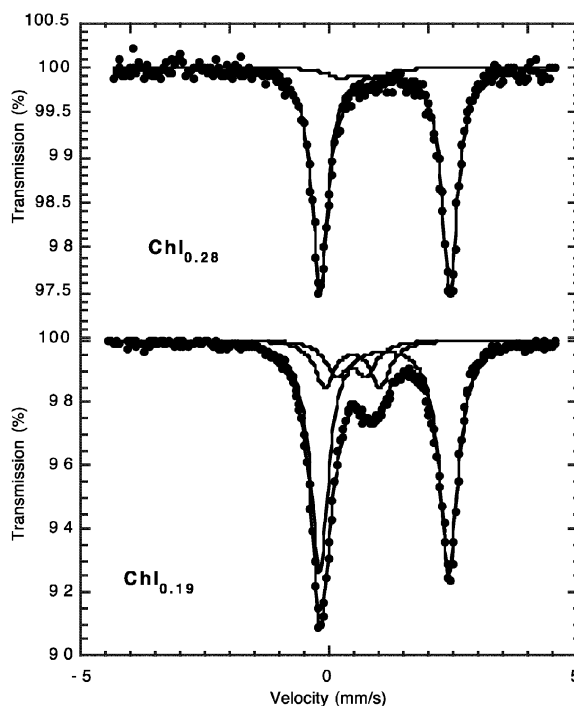

Figure 3. Room-temperature Mössbauer spectra of the two natural chlorites. The outer doublet corresponds to the Fe^{2+} octahedral site, whereas inner doublets represent Fe^{3+} octahedral sites (*cis*- and *trans*-configuration).

direction along the *c* axis. The refined cation-site occupancy factors accorded with the assumption that the chlorites are trioctahedral, but their large estimated standard deviations made it impossible to make further deductions from them. The unit-cell parameters obtained are given in Table 3.

Mössbauer spectroscopy

Mössbauer parameters of the natural chlorites are presented in Table 4 and the corresponding spectra are shown in Figure 3. The spectrum of $Chl_{0.28}(1.4)$ shows a clean symmetric doublet arising from Fe^{2+} in the octahedral environment. The line width is indicative of ferrous Fe in only one type of octahedral position, *i.e.* either *trans* or *cis* configuration. Additionally, absorption lines from ferric Fe are observed. The asymmetric shape and line width of the ferric Fe absorption peaks of sample $Chl_{0.19}(6.0)$ clearly show ferric Fe occupying at least two types of *trans* and *cis* octahedral co-ordination in the 2:1 layer (Annersten, 1974). The small isomer shift, 0.41 mm/s, would be Fe^{3+} in *trans* configuration in

agreement with the 2:1 layer in biotite (Annersten, 1974) and the larger isomer shift, 0.49 mm/s, is assigned to Fe^{3+} in *cis* configuration. Although Phillips *et al.* (1980) distributed all heavy elements (Fe^{3+}, Cr^{3+} and Ni^{2+}) in octahedral site *M*4 of the brucite-like sheet, there is no obvious absorption that can be assigned to ferric Fe in the brucite-like sheet in the present sample. Isomer shifts for such an absorption doublet is expected to show a smaller shift than 0.41 mm/s due to the smaller bonding distances in the *M*4 site (Joswig *et al.*, 1980). Employing three ferric Fe doublets led to a fit with larger χ^2 values and an absorption doublet with an isomer of shift of 0.37 mm/s.

^{29}Si *NMR*

Figure 4 shows ^{29}Si MAS spectra, acquired at 9.4 T, of polycrystalline powders of the two natural chlorites. The spectrum in (a) was acquired from $Chl_{0.28}(1.4)$ spinning at 7.5 kHz. It displays a strong peak at an isotropic chemical shift of −85 ppm, together with two weak sidebands. The anisotropy of the chemical shift

Table 3. Unit-cell parameters.

Sample	*a* (Å)	*b* (Å)	*c* (Å)	α (°)	β (°)	γ (°)	*V* (Å³)
ChlS	5.3172(6)	9.2123(9)	14.380(1)	90.286(2)	97.093(2)	90.007(2)	699.00
$Chl_{0.28}(1.4)$	5.3115(6)	9.206(1)	14.299(2)	90.410(2)	97.126(2)	90.045(2)	693.77
$Chl_{0.19}(6.0)$	5.328(1)	9.230(1)	14.427(5)	90.255(6)	97.083(8)	90.015(4)	704.06

Table 4. Room-temperature Mössbauer data.

Sample	Fe^{2+}				Fe^{3+}				Fe^{3+}/(Fe^{2+}+Fe^{3+})
	IS (mm/s)	ΔE_Q (mm/s)	FWHM (mm/s)	I (%)	IS (mm/s)	ΔE_Q/ mm/s	FWHM (mm/s)	I (%)	
Chl$_{0.28}$(1.4)	1.13	2.62	0.20	93.4	0.59	0.73	0.44	6.6	0.06
Chl$_{0.20}$(6.0)	1.11	2.60	0.23	70.6	0.41	0.77	0.36	12.6	0.29
					0.49	1.03	0.41	16.7	

Isomer shift (IS) and quadrupolar splittings (ΔE_Q) are within 0.01 mm/s and intensities (*I*) are within ±2%
FWHM = full peak width at half maximum height

interaction (CSA) generates a set of spinning sidebands under MAS conditions and its size may be extracted by fitting experimental spectra to numerically simulated ones. Typically, ^{29}Si chemical shift anisotropies are <100 ppm (Oldfield *et al.*, 1983). However, in samples containing significant amounts of paramagnetic species, the anisotropy of the magnetic susceptibility may also provide intense sideband formation (Grimmer *et al.*, 1983; Oldfield *et al.*, 1983). As in the case of CSA, the magnetic susceptibility tensor increases linearly with the external magnetic field, and the two anisotropies may therefore not be distinguished by comparing MAS spectra at different external magnetic fields (Oldfield *et al.*, 1983). Henceforth, we only consider their sum, which will be referred to as 'effective anisotropy'. For the ^{29}Si resonance from Chl$_{0.28}$(1.4) (Figure 4a), we estimated it as 105±7 ppm, with an accompanying asymmetry parameter <η < 0.4.

The sample Chl$_{0.19}$(6.0) has less Al substitution in the tetrahedral sheet, but a significantly larger amount of Fe compared to Chl$_{0.28}$(1.4). Figure 4b displays the MAS spectrum recorded at a spinning frequency of 8.0 kHz. It differs mainly in three features compared to that from

Figure 4. ^{29}Si MAS spectra recorded at a magnetic field of 9.4 T for the two natural chlorite samples. (a) Chl$_{0.28}$(1.4), spinning at 7.5 kHz. The spectrum resulted from 4096 accumulated signals transients. (b) Chl$_{0.19}$(6.0), 8.0 kHz spinning speed and 12288 transients. Each spectrum displays an intense centerband peak around (a) −85 ppm and (b) −90 ppm: all other peaks are spinning sidebands.

Chl$_{0.28}$(1.4). First, the centerband appears at a more shielded position (−90 ppm), as expected from the smaller amount of ^{IV}Al in the sample (Mägi *et al.*, 1984; Sanz and Serratosa, 1984). Further, the sample richer in Fe generates significantly broader NMR peaks, as well as more intense spinning sidebands. The effective anisotropy was estimated as ~205 ppm. We attribute both effects to the presence of a larger amount of Fe. In a relaxation study of a natural chlorite, Watanabe *et al.* (1983) attributed the extensive sideband formation to an unusually large ^{29}Si CSA alone, rather than from magnetic susceptibility, an interpretation supported by the absence of EPR signals from their sample. While the estimated anisotropy from Chl$_{0.28}$(1.4), which contains only 1.4 wt.% Fe$_2$O$_3$, could correspond to a large CSA interaction, the anisotropy of Chl$_{0.19}$(6.0) is more than twice as large as typical values of ^{29}Si chemical shift anisotropies. It is most likely that there are magnetic susceptibility contributions to both ^{29}Si spectra, and the value of 105 ppm should be regarded as the upper limit for ^{29}Si chemical shift anisotropies in chlorites.

Our ^{29}Si spectra agree with observations made in previous studies of paramagnetic minerals, *i.e.* that there is usually, but not always, a correlation between the paramagnetic content and spectral features like peak width and the number of spinning sidebands of significant amplitudes (Grimmer *et al.*, 1983; Morris *et al.*, 1990; Oldfield *et al.*, 1983). The extent of spectral broadening, as well as the effective anisotropy, correlates qualitatively with the Fe content of the corresponding minerals (Table 5). The content of Fe$_2$O$_3$ in Chl$_{0.19}$(6.0) is 4.2 times that of Chl$_{0.28}$(1.4). The peak width of Chl$_{0.19}$(6.0) is ~2.2 times greater than that of Chl$_{0.28}$(1.4) and the corresponding ratio between the effective anisotropies of the two samples is 2.0.

Figure 5 compares regions zoomed around the centerbands of ^{29}Si spectra recorded at two different external fields of 9.4 T and 4.7 T. The signals in Figure 5c−d are concentrated to each centerband, resulting both from the use of higher spinning frequency (12 kHz) and because the effective anisotropy at 4.7 T is only half of that at 9.4 T. Differences in line widths appear to be the main distinction between spectra at different fields. Full widths at half maximum height (FWHM) are given in Table 5 and were estimated
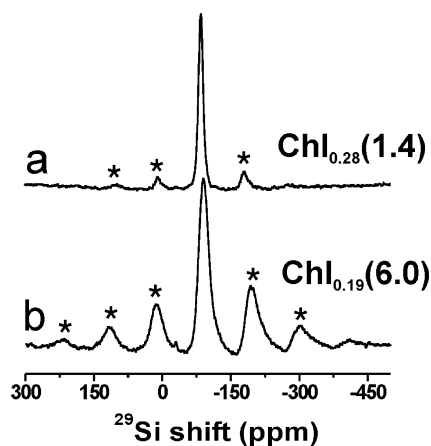
Table 5. ^{29}Si NMR parameters at external magnetic fields of 4.7 T and 9.4 T.

Sample	B_0 (T)	δ (ppm)[a]	FWHM (kHz)[b]	FWHM (ppm)[b]	Effective anisotropy (ppm)[c]
Chl$_{0.28}$(1.4)	9.4	-85.4 ± 0.8	0.98	12.3	~105
	4.7	-85.6 ± 0.4	0.505	12.7	
Chl$_{0.19}$(6.0)	9.4	-89.8 ± 1.0	2.1	26.9	~205
	4.7	-88.8 ± 0.8	1.25	31.4	

[a] Isotropic chemical shift, estimated from spectral peak amplitude maxima.
[b] Full width at half maximum height estimated directly from the MAS spectrum (no reference to a line-shape function).
[c] Effective anisotropy, given by the sum of contributions from CSA and magnetic susceptibility, determined from fitting the MAS sideband amplitudes at 9.4 T to numerical simulations.

directly from the MAS peaks as these lineshapes could not satisfactorily be fitted to single Gaussians, Lorentzians or mixtures thereof.

^{27}Al NMR

1D MAS. Regions zoomed around the center of the ^{27}Al MAS spectrum from each chlorite are shown in Figure 6. They display two main signals around 59−68 ppm and 8−10 ppm, corresponding to Al in tetrahedral and octahedral coordination, respectively. As ^{27}Al is a quadrupolar nucleus, its NMR peak position is given by the sum of isotropic chemical and second-order isotropic quadrupolar shifts (Lippmaa *et al.*, 1986; Smith, 1993), the latter depending on the external magnetic field employed. The isotropic chemical shifts are derived and discussed below. As in the case of ^{29}Si, the ^{27}Al line widths clearly also correlate with the amount of Fe in each sample: broadenings from second-order quadrupolar interactions (Lippmaa *et al.*, 1986; Smith, 1993) constitute the primary resolution-limiting factor only in the case of the Fe-free specimen, ChlS.

The distribution of Al between tetrahedral and octahedral sheets of the samples were estimated by calculating the ratio of their corresponding integrated intensities of ^{IV}Al and ^{VI}Al NMR signals: $R_{exp} = I[^{IV}Al]/I[^{VI}Al]$. These values may be compared with ^{IV}Al/^{VI}Al ratios calculated from the sample compositions, R_{calc} (see Table 6). For Chl$_{0.28}$(1.4) there is excellent agreement between the experimental (0.76) and calculated (0.80) ratios. However, they deviate more (by ~10%) for the Fe-richer mineral Chl$_{0.19}$(6.0). The problems of using solid-state NMR to obtain the relative amounts of tetrahedral and octahedral Al in the presence of significant amounts of paramagnetic ions (>3 wt.%) is well known and discussed in the literature (Grimmer *et al.*, 1983; Morris *et al.*, 1990; Oldfield *et al.*, 1983). On the other hand, the experimentally obtained ratio $R_{exp} = 0.727$ for the Fe-free specimen ChlS allowed us to deduce the formula of equation 4b. Given the absence of the main error source in quantifying the ^{IV}Al and ^{VI}Al signals, the accuracy of R_{exp} is expected to be better than ~4%, which is the error obtained in the case of Chl$_{0.28}$(1.4). However, this assumes no loss of elements during synthesis and that the sample is indeed phase-pure as indicated by XRD.

3QMAS. The two-dimensional MQMAS technique improves resolution in NMR spectra from half-integer quadrupolar nuclei, such as ^{27}Al. The resulting 2D spectrum displays the MAS spectrum along one dimension. *i.e.* the anisotropic dimension, and a high-resolution spectrum in the other, *i.e.* isotropic dimension
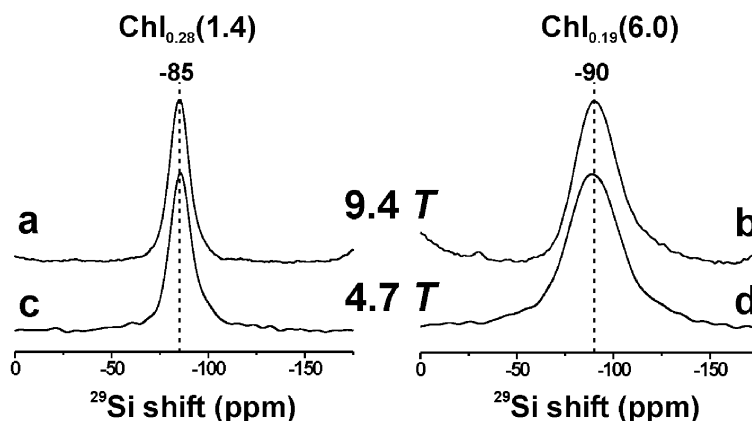

Figure 5. Zoomed regions around the centerbands of ^{29}Si MAS spectra recorded at 9.4 T and 4.7 T from Chl$_{0.28}$(1.4) (a,c) and Chl$_{0.19}$(6.0) (b,d).
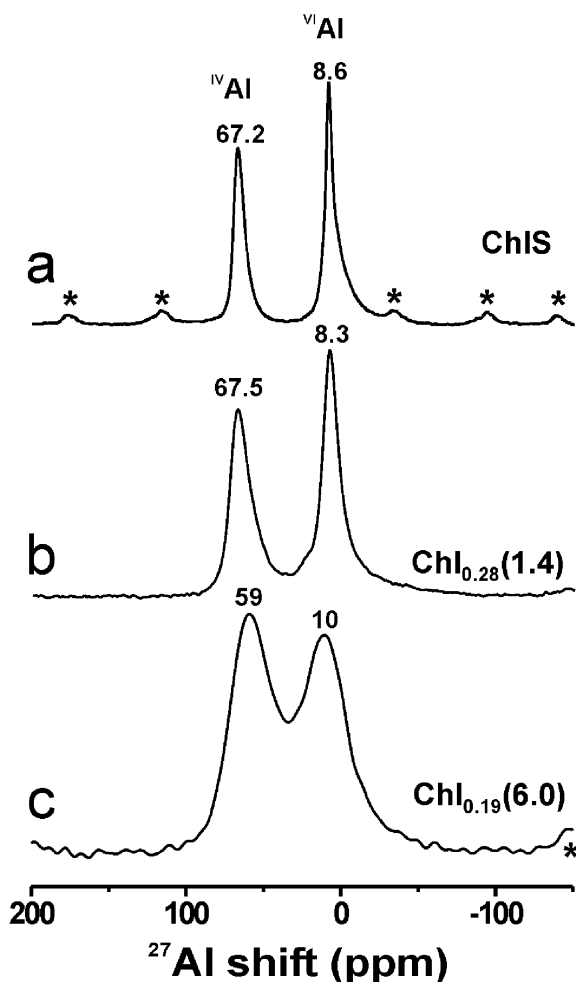
Figure 6. ^{27}Al MAS spectra recorded at 9.4 T for (a) ChlS, 10.99 kHz spinning frequency; (b) $Chl_{0.28}(1.4)$, 22.4 kHz; (c) $Chl_{0.19}(6.0)$, 22.0 kHz. The spectra were recorded using a 4 mm rotor (a) and 3.2 mm rotors (b,c), and resulted from summing (a) 624, (b) 1092, (c) 3072 signal transients. The ppm values at the peak maxima are displayed on top of each peak and asterisks indicate spinning sidebands.

(Frydman and Harwood, 1995). While ^{27}Al 3QMAS experiments on highly crystalline samples provide narrow peaks in the isotropic dimension, significantly broader signals result from samples possessing structural disorder. This is inherent to chlorites due to a distribution of Al and Si units in the tetrahedral sheets, as well as for Mg^{2+}, Al^{3+} and other octahedral cations. In such cases, the observed 2D peaks are tilted relative to the spectral axes: the degrees of distributions of ^{27}Al chemical shifts and quadrupolar couplings may be assessed by inspecting the resonance displacement directions along each spectral dimension. Further, in the case of Fe-containing chlorites, homogeneous line-broadening additionally decreases resolution.

Figure 7 shows ^{27}Al 3QMAS spectra from our chlorites. To emphasize the significant differences in line widths and resolution of the signals from the various samples, the spectra are displayed over equal frequency ranges, but the two different 3QMAS implementations used for recording the spectra are associated with different conventions in the definition of the ppm scale along the isotropic dimension, as explained by Man (1998). There are two crystallographically inequivalent sites in the tetrahedral sheet, and four inequivalent octahedral sites (two in the talc-like layer and two in the brucite-like sheet). In addition to clearly separating the ^{IV}Al and ^{VI}Al signals, the 3QMAS spectrum of ChlS (Figure 7a) also resolves two of the potentially four octahedral signals. As XRD did not indicate the presence of additional phases other than chlorite, we believe that this is the first demonstration of the discrimination of NMR signals from inequivalent octahedral Al sites in a phyllosilicate mineral. To our knowledge, only one report exists in the literature (about a montmorillonite) on the separation of tetrahedral Al signals (Ohkubo *et al.*, 2003).

We tentatively assign the narrow peak (denoted O in Table 6) to the *M4* site in the brucite-like sheet as it is the most symmetric of the four environments, while the broader peak may stem from overlapping signals of the

Table 6. ^{27}Al NMR parameters for ^{IV}Al and ^{VI}Al sites, denoted *T* and *O*, respectively, obtained from MAS and 3QMAS spectra at 9.4 T.

Sample		δ (ppm)[a]	δ_{iso} (ppm)	$C_{Q\eta}$ (MHz)	R_{exp}[b]	R_{calc}[c]
ChlS	T	67.2	71.7±1	3.2±0.2		
	O	8.6	10.7±1	2.2±0.2	0.727	–
	O2	–	14.5±1	4.0±0.2		
$Chl_{0.28}(1.4)$	T	67.5	73.0±1.5	3.0±0.3	0.764	0.797
	O	8.3	11.0±1.5	2.1±0.3		
$Chl_{0.19}(6.0)$	T	59.0	68.4±2	3.6±0.5	0.88	0.97
	O	10.6	12.2±2	2.4±0.5		

[a] Peak position determined directly from the 1D MAS spectrum, accurate to within ±0.5 ppm. Note that there are two octahedral sites resolved in the 3QMAS spectrum of ChlS, and the value 8.6 ppm is the peak maximum of their superposition.
[b] Ratio $R_{exp} = I(T)/I(O)$ from integrated intensities of the fitted peaks.
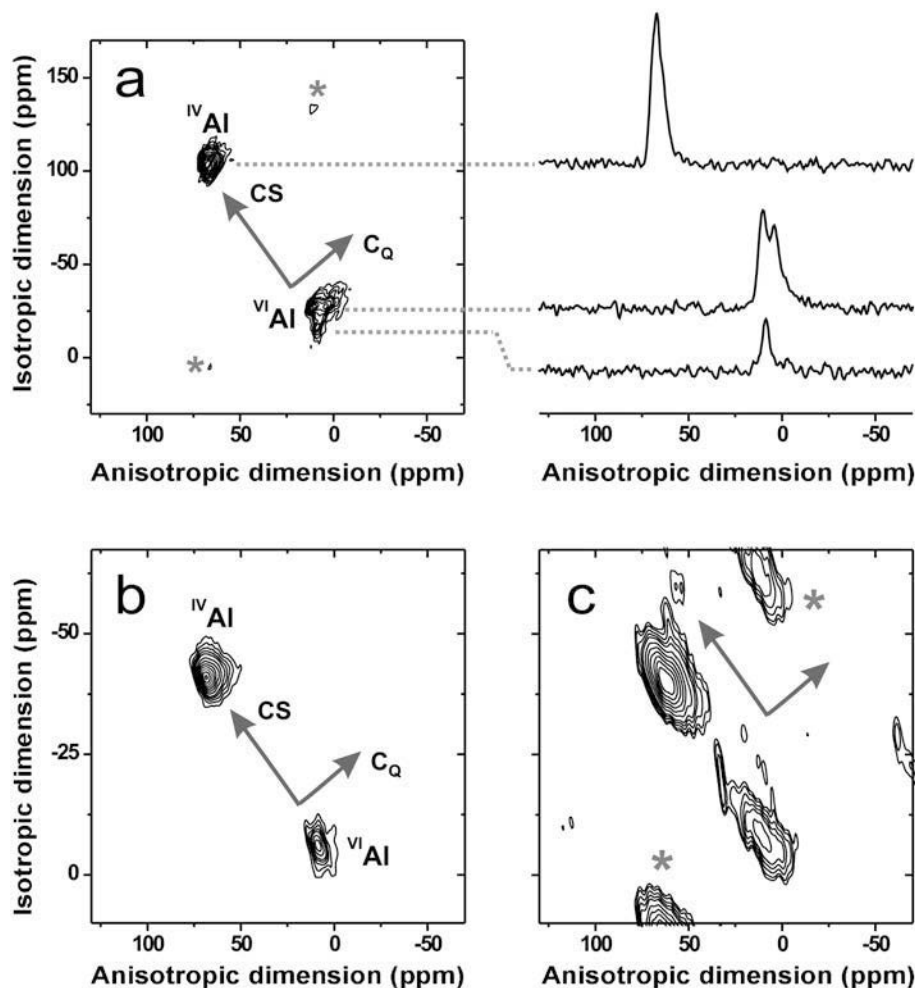[c] Ratio $I(T)/I(O)$ obtained from the chemical composition (equations 5−6)

Figure 7. (a) Shifted echo 3QMAS spectrum of the synthetic ChlS sample, spinning at 10.99 kHz. Shifted echo split-t_1 3QMAS spectra of (b) $Chl_{0.28}(1.4)$ (22.4 kHz spinning) and (c) $Chl_{0.19}(6.0)$ (14.0 kHz spinning). The centerband peak positions from the tetrahedral and octahedral sites are indicated. Sidebands are marked by asterisks. Contour levels were set at $10, 15, 20, 25, 30, 40, \cdots,$ 90%. The displacement directions expected from distributions of isotropic chemical shifts and quadrupolar coupling constants are indicated by arrows. The peak at the constant value ~30 ppm along the anisotropic dimension of (c) is an artifact at the position of the spectrometer carrier frequency.

more distorted octahedral environments, *i.e.* $M1$, $M2$ and $M3$. Interestingly, despite clear signs of distributions of quadrupolar coupling constants in the 2D spectrum (Figure 7a, left panel), the slice through the broader signal (Figure 7a, right panel) is not featureless, but could very well correspond to only one site, *i.e.* it is not obvious from the spectrum that this peak would stem from three overlapping signals. For instance, in the brucite-like sheet, R^{3+} ions such as Al^{3+} have a tendency to concentrate in the less distorted $M4$ site whereas R^{2+} prefers the $M3$ position, but the ordering varies in degree and is not always complete. Consequently, our results indicate that it is not obvious that all four inequivalent octahedral positions are occupied by Al. On the other hand, previous structure refinements have not revealed any evidence for ordering of the octahedrally coordinated cations in the talc-like layer (Bailey, 1988).

The peak from the octahedral site in $Chl_{0.28}(1.4)$, however, is homogeneously broadened to an extent that the separation of individual octahedral peaks is not possible (Figure 7b). The tetrahedral peak is clearly extending along the direction of chemical shift dispersion, indicating a higher degree of structural disorder in the tetrahedral sheet. For the Fe-richer sample $Chl_{0.19}(6.0)$ (Figure 7c), resolution is degraded further due to increased homogeneous broadening. This sample displays a more shielded ^{VI}Al signal and a less shielded ^{IV}Al signal compared to the other two samples. The reason may be additional paramagnetic shifts resulting from the larger amount of Fe (Grimmer *et al.*, 1983; Morris *et al.*, 1990; Oldfield *et al.*, 1983).

It is possible to extract the isotropic ^{27}Al chemical shift and the corresponding quadrupolar product ($C_{Q\eta}$) for each crystallographically inequivalent site resolved

in the 3QMAS spectrum. The quadrupolar product is given by

$$C_{Q\eta} = C_Q \sqrt{1 + \frac{\eta^2}{3}} \qquad (7)$$

where η is the asymmetry parameter of the electric field gradient (efg) tensor, and $C_Q = e^2qQ/h$ is the quadrupolar coupling constant, corresponding to the product of the nuclear quadrupole moment (eQ) and the largest pricipal value (eq) of the efg tensor. Note that in cases of non-resolved singularities of the MAS lineshapes (or insufficient S/N as in the case of the spectrum from ChlS), C_Q and η cannot be determined separately, although $C_{Q\eta}$ provides an upper limit for the quadrupolar coupling constant through the range of the asymmetry parameter ($0 \leqslant \eta \leqslant 1$), *i.e.* C_Q is constrained within $0.866C_{Q\eta} \leqslant C_Q \leqslant C_{Q\eta}$. From the 3QMAS spectra (Figure 7) we obtained the isotropic chemical shifts and quadrupolar products (Table 6) for the tetrahedral and octahedral Al sites from the center of gravities of the 2D spectral peaks, as discussed by Man (1998).

Tetrahedral cation ordering

The Al and Si tetrahedra are not randomly distributed over the tetrahedral sheets of phyllosilicates and the negative charge from AlO_4 units over the sheet is reduced locally by additional restrictions (Barron *et al.*, 1985; Dempsey, 1969; Herrero and Serratosa, 1989; Loewenstein, 1959). Different models have been proposed for distributing the negative charge. The most basic is that of Loewenstein (1959), according to which Al−O−Al linkages are excluded. Dempsey's rule (1969), also referred to as maximum dispersion of charges (MDC) (Herrero and Serratosa, 1989), is more restrictive as Al−O−Si−O−Al constellations are additionally minimized over the sheet. It has been found for several phyllosilicates that the Al distribution is more ordered than predicted from Loewenstein's rule, but less ordered than that of Dempsey. A model of homogeneous dispersion of charges (HDC) was generally shown to best reproduce experimental results (Herrero and Serratosa, 1989; Lausen *et al.*, 1999). In addition to Loewenstein's rule, the HDC model implies that Al is distributed as evenly as possible over each six-membered ring of the lattice, in practice resulting in the number of Al per hexagon being as close as possible to the ratio $x = n_{Al}/(n_{Al} + n_{Si})$. The ^{29}Si spectra of Welch *et al.* (1995) from two synthetic Fe-free chlorite specimens of tetrahedral sheet compositions $x = 0.25$ and $x = 0.36$ revealed resolved signals for each of the four $Q^3(mAl)$ units. The sample with least Al substitution was found to comply with the HDC model, whereas that with more substitution indicated higher Al ordering (Welch *et al.*, 1995).

Unfortunately, the severely broadened NMR peaks from natural chlorites present several challenges for

assigning, let alone quantifying, the ^{29}Si spectral components to their respective $Q^3(mAl)$ environments. As well as in the present study, previous ^{29}Si spectra for chlorites (Komarneni *et al.*, 1986; Nakata *et al.*, 1986; Watanabe *et al.*, 1983) displayed very broad peaks (>15 ppm FWHM), and at best one can seek relationships between the position of the peak maxima and the tetrahedral Al substitution parameter x. Weiss *et al.* (1987) reported ^{29}Si shifts from one natural chlorite. However, the Fe content of the sample was not indicated and the spectrum was not shown. From the overall displacement of the peak position of ~4.5 ppm in our $Chl_{0.28}(1.4)$ sample compared to that from $Chl_{0.19}(6.0)$ (Table 3) it may, however, be anticipated that each Si unit in the former specimen has, on average, one extra Al tetrahedron as nearest neighbor compared to $Chl_{0.19}(6.0)$.

In this section, we explore the limitations of ^{29}Si NMR as applied to natural chlorites. We constructed a set of ^{29}Si spectra over a compositional range of $0.1 < x < 0.5$, by assuming peaks with equal FWHM of 10 ppm, positioned at $Q^3(mAl)$ chemical shifts of −80 ($m = 3$), −83.5 ($m = 2$), −87.5 ($m = 1$) and −91 ($m = 0$) ppm, respectively. These shifts were obtained from the mean values of the experimental shifts obtained by Welch *et al.* (1995), while the relative abundances of the $Q^3(mAl)$ environments were obtained numerically as follows; n "fictitious" Al atoms and ($N-n$) Si atoms were distributed over an N-site hexagonal grid, implemented with periodic boundary conditions, to emulate the set of tetrahedral centers of one chlorite tetrahedral sheet (see Figure 1c). Then, the number of possible ways of distributing the fictitious atoms was calculated according to the restrictions imposed either by Loewenstein's or Dempsey's rules. The relative abundance of each $Q^3(mAl)$ unit was determined from the ratio between the number of possible ways to form this environment relative to the total number of possible atomic constellations over the grid. The calculations were repeated for n taking integers in the range $1 \leqslant n \leqslant N/2$ in the case of Loewenstein's rule, whereas those involving Dempsey's rule were only taken up to the limiting composition $x = 0.25$, beyond which Al−Si−Al unit connectivities cannot be strictly avoided (Herrero and Serratosa, 1989). The resulting relative abundances of the various $Q^3(mAl)$ environments are directly proportional to the corresponding NMR spectral amplitudes deriving from the ^{29}Si nuclei of these units.

While the fairly computer-intensive calculations prevented us from obtaining 'exact' $Q^3(mAl)$ amplitudes, we inspected their convergence by comparing the results from calculations involving $N = 16, 24, 32$ and 40 atoms. The accuracies of the amplitudes presented below were estimated by comparing the deviations between the results of the two largest grids. The fastest convergences were obtained for compositions in the range $x < 0.25$, giving errors <3% for each $Q^3(mAl)$ amplitude. The least

accurate results were obtained for $x = 0.38$, for which the maximum error was ~7.5%. This is sufficient for the present discussion.

Figure 8 shows the spectrum of each set of $Q^3(m\mathrm{Al})$ amplitudes, as well as their sum for various values of x. Compare, for example, the experimental $^{29}\mathrm{Si}$ peak positions from $\mathrm{Chl}_{0.28}(1.4)$ and $\mathrm{Chl}_{0.19}(6.0)$ with the calculated ones: the latter reproduce qualitatively the experimental trend of higher deshielding for increasing x, although the calculations predict a smaller difference than observed experimentally. It should be noted that discrepancies between experimental and calculated peak maxima stem inevitably from the facts that the chemical shift of each $Q^3(m\mathrm{Al})$ unit is itself slightly dependent on x (this dependence is *a priori* unknown) and that the

peak widths of distinct units are, in practice, not necessarily equal [see, for example, Fig. 1 of Welch *et al.* (1995)]. However, by comparing the results from the Loewenstein and Dempsey distribution models for $x = 0.19$, it is impossible to say anything about the Si-Al ordering in the $\mathrm{Chl}_{0.19}(6.0)$ sample as the broad peak widths of the individual $Q^3(m\mathrm{Al})$ components combine into an overall featureless line. It should be noted that the limited spectral resolution from the synthetic minerals presented by Welch *et al.* (1995) results solely from atomic disorder. Hence, the results of our calculations are discouraging for the feasibility of determining tetrahedral cation distributions in any natural chlorite by NMR, as additional broadening from even minute amounts of paramagnetic species is sufficient to degrade
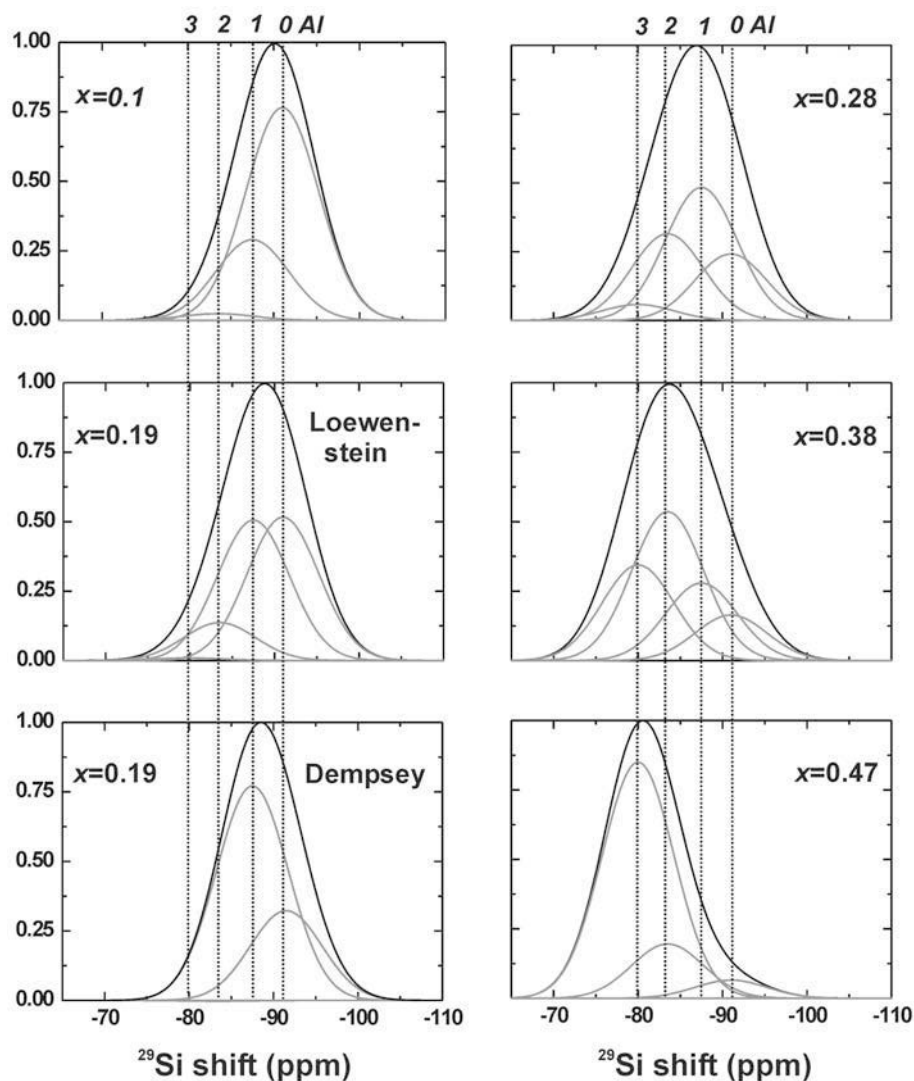

Figure 8. Calculated $^{29}\mathrm{Si}$ spectra based on the distributions of $Q^3(m\mathrm{Al})$ tetrahedral units according to the Loewenstein model for values of $x = n_{\mathrm{Al}}/(n_{\mathrm{Al}} + n_{\mathrm{Si}})$ indicated in each plot. For $x = 0.19$, the result of the Dempsey distribution is also shown. The four possible values for m are indicated at the top of each panel, and the grey lines represent the corresponding NMR peaks, having a FWHM width of 10 ppm and positioned at the following $^{29}\mathrm{Si}$ chemical shifts: $Q^3(0\mathrm{Al})$: −91.5 ppm; $Q^3(1\mathrm{Al})$: −87.5 ppm; $Q^3(2\mathrm{Al})$: −83.5 ppm and $Q^3(3\mathrm{Al})$: −80.0 ppm. The black lines show the resulting peaks, normalized such that each maximum amplitude is 1.

spectral resolution such that comparisons between experiments and calculations are not possible.

CONCLUSIONS

The powder XRD patterns ascertained that our chlorite samples are essentially mono-mineralic, and the Mössbauer spectra indicated that Fe is exclusively in octahedral coordination. We have reported isotropic ^{29}Si and ^{27}Al NMR chemical shifts, to our knowledge for the first time in the case of ^{27}Al. The presence of relatively large amounts of paramagnetic species in the natural samples resulted in broad ^{29}Si peaks. Whereas the ^{29}Si spectral peak positions did correlate with the amount of Al in the tetrahedral sheets, very limited detailed information of Al-Si ordering is to be expected from NMR studies on natural chlorites. However, as demonstrated by Welch *et al.* (1995), very accurate ordering information is provided by synthetic Fe-free samples. As even minute amounts of Fe (typically >0.5 wt.%) prevent estimation of the relative $Q^3(m$Al$)$ intensities, we believe that future solid-state NMR studies should employ synthetic chlorites as models for natural minerals.

This is also corroborated by the ^{27}Al 3QMAS NMR experiments on the synthetic ChlS sample, which allowed us to resolve two signals out of the potentially four inequivalent octahedral sites. As they are associated with quite different quadrupolar coupling constants, ~2 and ~4 MHz, respectively, we tentatively attribute the former signal to the highly symmetric M4 site in the brucite-like sheet and the latter as stemming from overlapping signals from M3 in the brucite-like sheet, and M1 and M2 of the talc-like layer. To our knowledge, this is the first report of the discrimination of crystallographically inequivalent octahedral Al sites by NMR on phyllosilicates.

These results indicate that the application of MQMAS (Frydman and Harwood, 1995) at higher magnetic fields, in conjunction with ^{1}H-^{27}Al cross-polarization for spectral editing (based on the varying degree of proximity of Al to OH groups) may allow for further resolution enhancements. This is a promising line of investigation to identify crystallographically inequivalent sites in phyllosilicates.

ACKNOWLEDGMENTS

REFERENCES

Annersten, H. (1974) Mössbauer studies of biotites. *American Mineralogist*, **59**, 143−151.

Bailey, S.W. (1980) Structures of layer silicates. Pp. 1−123 in: *Crystal Structures of Clay Minerals and their X-ray Identification* (G.W. Brindley and G. Brown, editors). Monograph **5**, Mineralogical Society, London.

Bailey, S.W. (1988) Chlorites: structures and crystal chemistry. Pp. 347−403 in: *Hydrous Phyllosilicates (Exclusive of Micas)*. (S.W. Bailey, editor). Reviews in Mineralogy, **19**. Mineralogical Society of America, Washington, D.C.

Bailey, S.W., Brindley, G.W., Johns, W.D., Martin, R.T. and Ross, M. (1971) Summary of national and international recommendations on clay mineral nomenclature by 1969−1970. Clay Minerals Society Nomenclature Committee. *Clays and Clay Minerals*, **64**, 129−132.

Barron, P.F., Slade, P. and Frost, R.L. (1985) Ordering of aluminum in tetrahedral sites in mixed-layer 2:1 phyllosilicates by solid-state high-resolution NMR. *Journal of Physical Chemistry*, **89**, 3880−3885.

Brandt, F., Bosbach, D., Krawczyk-Bärsch, E., Arnold, T. and Bernhard, G. (2003) Chlorite dissolution in the acid pH-range: a combined microscopic and macroscopic approach. *Geochimica et Cosmochimica Acta* **67**, 1451−1461.

Brindley, G.W. and Brown, G. (1984) *Crystal Structures of Clay Minerals and their X-ray Identification* (G.W. Brindley and G. Brown, editors). Monograph **5**. Mineralogical Society, London.

Brown, S.P. and Wimperis, S. (1997) Two-dimensional multiple-quantum MAS NMR of quadrupolar nuclei: A comparison of methods. *Journal of Magnetic Resonance*, **128**, 42−61.

Dempsey, E. (1969) The calculation of Madelung potentials for Faujasite-type zeolites. I. *Journal of Physical Chemistry*, **73**, 3660−3668.

Ericsson, T. and Wäppling, R. (1976) Texture effects in 3/2−1/2 Mössbauer spectra. *Journal de Physic, Colloque C6 supplement*, **12**, 719−723.

Ferrow, E. and Roots, M. (1989) A preparation technique for TEM specimens: application to synthetic Mg-chlorite. *European Journal of Mineralogy*, **1**, 815−819.

Foster, M.D. (1962) Interpretation of the composition and a classification of chlorites. *US Geological Survey, Professional Paper*, **414-A**, 1−33.

Frydman, L. and Harwood, J.S. (1995) Isotropic spectra of half-integer quadrupolar spins from bidimensional Magic-Angle Spinning NMR. *Journal of the American Chemical Society*, **117**, 5367−5368.

Grimmer, A., Lampe, F., Mägi, M. and Lippmaa, E. (1983) Hochauflösende ^{29}Si-NMR and festen Silicaten; Einfluß von Fe^{2+} in olivinen. *Zeitschrift für Chemie*, **23**, 343−344.

Herrero, C.P. and Serratosa, J.M. (1989) Dispersion of charge deficits in the tetrahedral sheet of phyllosilicates. Analysis from ^{29}NMR spectra. *Journal of Physical Chemistry*, **93**, 4311−4315.

Johansson, K.E., Palm, T. and Werner, P.-E. (1980) An automatiac microdensitometer for X-ray powder diffraction photographs. *Journal of Physics E: Scientific Instruments*, **13**, 1289−1291.

Joswig, W., Fuess, H., Rothbauer, R., Takéuchi, Y. and Mason, S.A. (1980) A neutron diffraction study of a one-layer triclinic chlorite (pennite). *American Mineralogist*, **65**, 349−352.

Klein, C. (2002) *The 22nd edition of the Manual of Mineral Science*. John Wiley & Sons, Inc., New Jersey, 641 pp.

Komarneni, S., Fyfe, C.A., Kennedy, G.J. and Strobl, H. (1986) Characterization of synthetic and naturally occurring clays

by ^{27}Al and ^{29}Si magic-angle-spinning NMR spectroscopy. *Journal of the American Ceramic Society*, **69**, C-45−C-47.

Lausen, S.K., Lindgreen, H., Jakobsen, H.J. and Nielsen, N.C. (1999) Solid-state ^{29}Si MAS NMR studies of illite and illite-smectite from shale. *American Mineralogist*, **84**, 1433−1438.

Levitt, M.H. (1997) The signs of frequencies and phases in NMR. *Journal of Magnetic Resonance*, **126**, 164−182.

Lippmaa, E., Samoson, A. and Mägi, M. (1986) High-resolution ^{27}Al NMR of aluminosilicates. *Journal of the American Chemical Society*, **108**, 1730−1735.

Loewenstein, W. (1959) The distribution of aluminum in the tetrahedra of silicates and aluminates. *American Mineralogist*, **39**, 92−96.

Lougear, A., Grodzicki, M., Bertoldi, C., Trautwein, A.X., Steiner, K. and Amthauer, G. (2000) Mössbauer and molecular orbital study of chlorites. *Physics and Chemistry of Minerals*, **27**, 258−269.

Madhu, P.K., Goldbourt, A., Frydman, L. and Vega, S. (1999) Sensitivity enhancement of the MQMAS NMR experiment by fast amplitude modulation of the pulses. *Chemical Physics Letters*, **307**, 41−47.

Man, P.P. (1998) Scaling and labeling the high-resolution isotropic axis of two-dimensional multiple-quantum magic-angle-spinning spectra of half-integer quadrupole spins. *Physical Review B*, **58**, 2764−2782.

Massiot, D., Touzo, B., Trumeau, D., Coutures, J.P., Virlet, J., Florian, P. and Grandinetti, P.J. (1996) Two-dimensional magic-angle spinning isotropic reconstruction sequences for quadrupolar nuclei. *Solid State Nuclear Magnetic Resonance* **6**, 73−83.

Moore, D.M. and Reynolds, R.C., Jr. (1997) *X-ray Diffraction and the Identification and Analysis of Clay Minerals*. Oxford University Press, New York, 378 pp.

Morris, H.D., Bank, S. and Ellis, P.D. (1990) ^{27}Al NMR spectroscopy of iron-bearing montmorillonite clays. *Journal of Physical Chemistry*, **94**, 3121−3129.

Mägi, M., Lippmaa, E., Samoson, A., Engelhardt, G. and Grimmer, A.-R. (1984) Solid-state high-resolution silicon-29 chemical shifts in silicates. *Journal of Physical Chemistry*, **88**, 1518−1522.

Nagy, K.L. (1995) Dissolution and precipitation kinetics of sheet silicates. Pp. 173−233 in: *Chemical Weathering Rates of Silicate Minerals* (P.H. Ribbe, editor). Reviews in Mineralogy, **31**. Mineralogical Society of America, Washington, D.C.

Nakata, S., Asaoka, S., Tadami, K. and Takahashi, H. (1986) Characterization of natural zeolites and clays by high-resolution solid-state NMR. *Nendo-Kagaku* **26**, 197−208.

Newman, A.C.D. and Brown, G. (1987) The chemical constitution of clay. Pp. 1−128 in: *Chemistry of Clays and Clay Minerals* (A.C.D. Newman, editor). Longman Scientific and Technical, Essex, UK.

Ohkubo, T., Kanehashi, K., Saito, K. and Ikeda, Y. (2003) Observation of two 4-coordinated Al sites in montmorillonite using high magnetic field strength ^{27}Al MQMAS NMR. *Clays and Clay Minerals* **51**, 513−518.

Oldfield, E., Kinsey, R.A., Smith, K.A., Nichols, J.A. and Kirkpatrick, J.R. (1983) High-resolution NMR of inorganic solids. Influence of magnetic centers on magic-angle sample spinning lineshapes in some natural aluminosilicates. *Journal of Magnetic Resonance*, **51**, 325−329.

Phillips, T.L., Loveless, J.K. and Bailey, S.W. (1980) Cr^{3+} coordination in chlorites: a structural study of ten chromian chlorites. *American Mineralogist*, **65** 112−122.

Rodriguez-Carjaval, J. (2002) Fullprof_2000 [http://www-llb.cea.fr/fullweb/fp2k/fp2k_intro.htm]. Published online by Leon Brilloin.

Sanz, J. and Serratosa, J.M. (1984) ^{29}Si and ^{27}Al high-resolution MAS-NMR spectra of phyllosilicates. *Journal of the American Chemical Society*, **106**, 4790−4793.

Smith, M.E. (1993) Application of ^{27}Al NMR techniques to structure determination in solids. *Applied Magnetic Resonance*, **34**, 159−201.

Watanabe, T., Shimizu, H., Masuda, A. and Saito, H. (1983) Studies of ^{29}Si spin-lattice relaxation times and paramagnetic impurities in clay minerals by magic-angle spinning ^{29}Si-NMR and EPR. *Chemistry Letters*, **8**, 1293−1296.

Weiss, C.A. Jr., Altaner, S.P.J. and Kirkpatrick, R.J. (1987) High-resolution ^{29}Si NMR spectroscopy of 2:1 layer silicates: Correlations among chemical shift, structural distortions and chemical variations. *American Mineralogist*, **72**, 935−942.

Welch, M.D., Barras J. and Klinowski, J. (1995) A multi-nuclear NMR study of clinochlore. *American Mineralogist*, **80**, 441−447.